# Energy spectrum for a fractal lattice in a magnetic field

Jayanth R. Banavar
*Schlumberger-Doll Research, Old Quarry Road, Ridgefield, Connecticut 06877-4108*

Leo Kadanoff
*Department of Physics, University of Chicago, Chicago, Illinois 60637*

A. M. M. Pruisken*
*Schlumberger-Doll Research, Old Quarry Road, Ridgefield, Connecticut 06877-4108*

(Received 10 September 1984)

To simulate a kind of magnetic field in a fractal environment we study the tight-binding Schrödinger equation on a Sierpinski gasket. The magnetic field is represented by the introduction of a phase onto each hopping matrix element. The energy levels can then be determined by either direct diagonalization or recursive methods. The introduction of a phase breaks all the degeneracies which exist in and dominate the zero-field solution. The spectrum in the field may be viewed as considerably broader than the spectrum with no field. A novel feature of the recursion relations is that it leads to a power-law behavior of the escape rate. Green's-function arguments suggest that a majority of the eigenstates are truly extended despite the finite order of ramification of the fractal lattice.

## I. INTRODUCTION

Hamiltonians defined on fractal surfaces have been the subject of many papers lately.[1-8] In particular, Domany *et al.*[1] have given a detailed analysis of the spectrum of eigenstates of the Schrödinger equation defined on a two-dimensional (2D) Sierpinski gasket. This calculation is based upon exact decimination techniques which provide a powerful semianalytical method of finding detailed properties of the Hamiltonian.

Problems of fractal lattices are reminiscent of (but very much simpler than) those which are conventionally studied for electron localization. For this situation the localization can be rather fully understood. One learns, for example, that, although there are a few extended states, most states are very highly localized, on finitely ramified fractals. Furthermore, almost all the states have a very high degree of degeneracy. Of course, the observed localization phenomena on these systems are fundamentally different from Anderson localization. For one thing, these lattices give a finite order of ramification. For another, if one chooses to describe the self-similar structure by configurational disorder (e.g., by cutting some bonds) then the resulting "disorder" is highly correlated. Nonetheless, these systems form interesting test cases which are worth studying.

In this paper we study magnetic field effects on electronic motion through a 2D Sierpinski gasket (Fig. 1). Following Alexander,[6] we describe the motion by giving an electronic wave function at each mode of the lattice, $\psi_j$. The tight-binding Hamiltonian fixes the hopping matrix element between neighboring sites to have a magnitude $|f|$ which is the same for all nearest-neighbor sites and zero otherwise. A magnetic field is defined by giving the value of the phase on each bond so that the sum of phases along a closed path is the magnetic flux enclosed by the path.

The very simplest model is chosen by taking all bonds to have exactly the same phase. We make this choice by allowing all bonds in the direction of the arrows in Fig. 1 to have a matrix element $f=f_0e^{i\phi}$, and all bonds opposite to the arrows to have $\bar{f}=f_0e^{-i\phi}$, with $f_0$ real and positive. Although this choice gives a natural bond pattern, the magnetic flux pattern is far less natural. All the elementary upward-pointing triangles, like those labeled $A$ in the figure, have the very same flux, $\Phi_A=3\phi$. However, using the same convention for the sign of the flux, the smallest downward-pointing triangles labeled $B$ have flux $\Phi_B=-3\phi$, while larger downward-pointing triangles have larger negative flux, for example, $\Phi_C=-6\phi$. Hence, the magnetic field pattern studied is quite nontrivial.

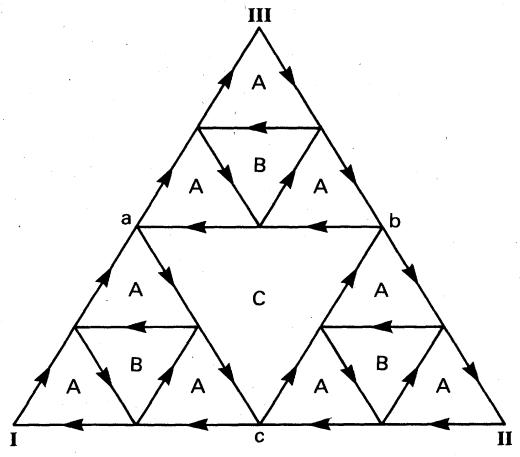


FIG. 1. Fragment of the Sierpinski gasket. The phase of the hopping matrix is equal to $\phi$ in the direction of the arrow and $-\phi$ otherwise.

 

Alexander[6] has studied more general flux patterns. We choose the pattern described above because it gives the simplest recursion equations and a maximum spatial homogeneity in $f$. Since the most interesting real magnetic field problem (the one in two dimensions) can be described as having a similarly spatially uniform $f$, we hope that our choice might lead to particularly interesting and perhaps extendable results.

This paper is organized as follows. In Sec. II we derive the recursion relations for the problem using a functional integral method. In Sec. III we study this map in a phenomenological manner. It turns out that the concept of "escape"[9,10] can be successfully employed in order to reveal the nature of the spectrum of eigenstates. A novel aspect is a power-law behavior of the escape, something which has not been observed before. This behavior is closely related to the occurrence of marginal behavior in the recursion relations in the neighborhood of a fixed line. On that fixed line the recursion relations reduce to a logistic map[11,12] with May-Feigenbaum parameter $\lambda=4$. From these notions the qualitative nature of the spectrum and of the eigenstates can be derived. The latter will be subject of Sec. IV (numerical studies).

In Sec. V we present arguments, using Green's functions, that a majority of the eigenstates are, indeed, truly extended. This is a quantum-mechanical result which is contrary to the "intuition" gained by studying classical problems on the gasket. Classically, the finite order of ramification of the gasket enables one to construct domains of arbitrary size having a constant domain-wall energy. As a result, for example, an Ising model on a gasket[13] has a $T_c$ of zero. In contrast, in our quantum problem, resonance effects permit a few links to produce a large coherence length.

## II. FORMULATION

### A. Decimation

Consider the partition function

$$Z(\epsilon)=\int D[\psi]D[\bar{\psi}]\exp[\bar{\psi}(\epsilon\underline{1}-H)\psi]=\det(\epsilon\underline{1}-H)\ , \tag{1}$$

where $\bar{\psi}=i\psi^{\dagger}$ and the integration is over complex Grassmann fields. In Eq. (1), $\epsilon$ denotes a trial value of the energy. Each actual eigenenergy $\epsilon_\alpha$ is a zero of the partition function. The partition function itself is simply a product of $\epsilon-\epsilon_\alpha$. For example, in the case of a trivial gasket with three sites (Fig. 2), we have

$$Z_0(\epsilon)=\det(\epsilon\underline{1}-H_0)\ , \tag{2}$$

where $H_0$ is given by

$$H_0=\begin{bmatrix} 0 & f & f^* \\ f^* & 0 & f \\ f & f^* & 0 \end{bmatrix}\ , \tag{3}$$

and $\underline{1}$ is a $3\times3$ unit matrix. This result is easily evaluated as

$$Z_0(\epsilon)=\epsilon^3-3\epsilon ff^*-f^3-(f^*)^3\ . \tag{4}$$

In our actual work we shall measure $\epsilon$ in units of the magnitude of the hopping, choosing as our variables $\phi$ and $x=\epsilon/|f|$. In terms of these variables, the basic partition function (4) becomes

$$D(x,\phi)=x^3-3x-2\cos3\phi\ . \tag{5}$$

On the trivial lattice, the eigenenergies are given in units of $|f|$ by the zeros of $D(x,\phi)$.

To elucidate the behavior of the nontrivial lattice, one performs a decimation procedure on it to eliminate sites until the trivial problem is reached. However, the coupling to the outside corners of the largest triangle may have to be handled separately since these sites are likely to have a special environment. We return to this point below, after the recursion relation for the other bonds is established.

The decimation is easily obtained as follows (see Fig. 3). The right-hand side of the figure is obtained from the left-hand side by eliminating sites $a$, $b$, and $c$, i.e., the fields $\psi$ on sites $a$, $b$, and $c$ are simply integrated out. The part of the Lagrangian corresponding to the left-hand side of Fig. 3 can be written as

$$L_{\text{block}}=[\bar{\psi}_i,\bar{\psi}_0]\begin{bmatrix} \epsilon-H_0 & -H_0 \\ -H_0 & \epsilon/2 \end{bmatrix}\begin{bmatrix} \psi_i \\ \psi_0 \end{bmatrix}\ , \tag{6}$$

where

$$[\psi_i,\psi_0]=[\psi_a\psi_b\psi_c,\ \psi_1\psi_2\psi_3]\ , \tag{7}$$

and $H_0$ is given by Eq. (3). The decimation, i.e., the integration over $\psi_i$, is easily performed, leading to a transformed Lagrangian for the block

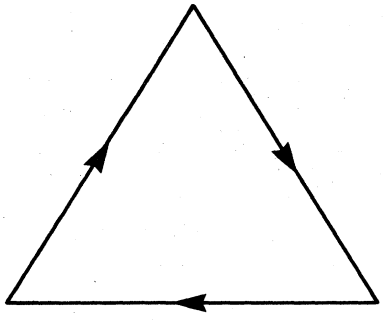

FIG. 2. The trivial lattice.

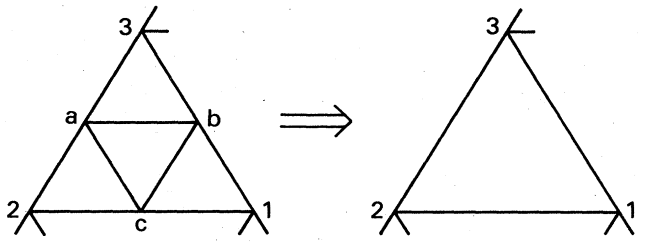


FIG. 3. Decimation consists of integration over Grassmann fields at sites $a$, $b$, and $c$, leading to effective hopping matrix elements between sites 1, 2, and 3.

$$L'_{\text{block}}=\bar{\psi}_0\left[\frac{x}{2}-\frac{H_0^2}{x-H_0}\right]\psi_0+\ln\det(x-H_0)\ , \tag{8}$$

where a $3\times3$ unit matrix is contained in $x$. Thus, if $H'_0$ represents a matrix just like $H_0$ of Eq. (3), except that $f$ is replaced by $f'$, we have generated new couplings $\epsilon'$ and $H'_0$ given by

$$\epsilon'/2-H'_0=\epsilon/2-H_0(\epsilon-H_0)^{-1}H_0\ .$$

By using the eigenstates of $H_0$, one can reduce these statements to the algebraic equations

$$\epsilon'-2(f'\Lambda+f'^*\Lambda^*)=\epsilon-\frac{2(f\Lambda+f^*\Lambda^*)^2}{\epsilon-f\Lambda-f^*\Lambda^*}\ . \tag{9}$$

Equation (9) represents three algebraic equations, obtained, respectively, by substituting for $\Lambda$ one of the three cube roots of unity. We solve these equations for $x'=\epsilon'/|f'|$ and $\phi'$ to find the recursion relations

$$x'=\frac{x(x^3-7x-6\cos3\phi)}{\Gamma^{1/2}\text{sgn}N}\ ,$$

$$N=x^2\cos2\phi+3x\cos\phi+\cos2\phi+\cos4\phi\ , \tag{10}$$

$$\Gamma=x^4+6x^3\cos3\phi+x^2(11+2\cos6\phi)+12x\cos3\phi+2+2\cos6\phi\ ,$$

$$\tan\phi'=-T/N,\quad T=x^2\sin\phi-3x\sin\phi+\sin2\phi-\sin4\phi\ . \tag{11}$$

There are two apparent ambiguities in these recursion equations: The sign of $x'$ is undetermined, and $\phi'$ can be displaced by 180° without affecting Eq. (11). Recursion relation (9) indicates that the correct choice is to let $\phi$ lie in the interval $[-90°,90°]$, while the sgn of the denominator in $x$ is always chosen to be the sgn of $N$, as in Eq. (10). We formally summarize recursion relations (10) and (11) by writing the result as a two-component function of two variables,

$$(x',\phi')=R(x,\phi)\ . \tag{12}$$

### B. Boundary conditions

One can visualize several different ways in which triangles like the one in Fig. 1 might be tied together. From the analytical point of view the simplest case is the one in which two triangles identical to the one shown in Fig. 1 touch at the three outside vertices, I, II, and III. These two large triangles are linked because the wave functions at I, II, and III are identical. This kind of boundary condition was introduced in Ref. 1.

For this situation the entire recursion procedure is simple. Start on a lattice with $(3^n+3)/2$ sites (counting both large triangles). For example, Fig. 1 depicts a case in which one major triangle of the $n=3$ problem is shown. Let the initial couplings be given by $x_n,\phi_n$. One then uses Eq. (12) to calculate effective couplings for the decimated system, i.e.,

$$(x_{j-1},\phi_{j-1})=R(x_j,\phi_j),\quad j=n,n-1,\ldots,2\ . \tag{13}$$

In this case all sites and bonds are equivalent so no special handling of the corner sites is necessary. Finally, the $n=1$ problem has two identical triangles put together and three possible eigenvalues,

$$x_1=4\cos(\phi_1+2\pi l/3),\quad l=0,1,2\ . \tag{14}$$

We describe this situation as obeying the "doubling" boundary condition. Given an initial value of magnetic field (hence $\phi$) and the coupling strength $f$, $\epsilon$ will be an eigenvalue of the gasket problem if

$$(x_1,\phi_1)=R^{n-1}(\epsilon/f_0,\phi) \tag{15}$$

obeys one of the three equations (14).

Alternatively, it is possible to fit the two largest triangles together in another way. Let the triangles not be identical but instead parity images of one another. Thus where one triangle has the bond $f_0e^{i\phi}$, the other has $f_0e^{-i\phi}$. We describe this situation as the "flipped doubling" boundary condition since it can be obtained from the previous one by flipping over one of the largest triangles. The same calculational method works, except that to describe the behavior of the $n=1$ triangles one has, instead of Eq. (14),

$$x_1=4(\cos\phi_1)(\cos2\pi l/3),\quad l=0,1,2\ . \tag{16}$$

Next consider the situation in which there is only the one main triangle shown in Fig. 1. The outside corners, labeled I, II, and III, each have only two nearest neighbors, while all other sites have four. Hence the on-site energies on these special sites behave differently. To describe this difference, let $y_j/x_j$ be the ratio of the on-site energy at the special sites to the on-site energy on the other sites for a large triangle with $(3^j+3)/2$ sites. As before, $(x_{j-1},\phi_{j-1})$ for $j=n,n-1,\ldots,2$ are given by Eq. (13). In addition, one has the determination of $y_j$, namely

$$y_{j-1}/x_{j-1}=g(y_j,x_j,\phi_j)\ , \tag{17a}$$

with

$$g(y,x,\phi)=\frac{y(x^3-3x-2\cos3\phi)-2x(x+\cos3\phi)}{x(x^3-7x-6\cos3\phi)}\ , \tag{17b}$$

and with the initial condition $y_n=x_n$. Finally, once one has found $\phi_1$, $x_1$, and $y_1$, one determines whether or not the original $\epsilon=f_0x$ is an eigenvalue by asking whether the level-1 triangle is at an eigenvalue, namely whether

$$y_1=2\cos(\phi_1+2\pi l/3),\quad l=0,1,2 \tag{17c}$$

corresponding to free boundary conditions.

The special symmetry of this gasket with free boundary conditions allows one to explicitly determine the eigenvalues and functions of the stage-$n$ gasket from those of a stage-$(n-1)$ gasket with three different boundary conditions. These different boundary conditions can be visualized in Fig. 1. The gasket is invariant under a rotation of $2\pi/3$. Therefore, all the eigenfunctions $\psi$ can be classified into three categories: They transform under such a rotation as $\psi\rightarrow e^{i\theta}\psi$ with $\theta=2\pi l/3$, $l=0,1,2$. Hence, one can construct the states of the gasket shown in Fig. 1 and those of the smaller gasket having I, $a$, and $c$ as its corners as follows: We let I be "free," and require that the wave functions at $a$ and $c$ be identical except for a

phase difference of $2\pi l/3$, $l=0,1,2$. The eigenvalues thus obtained are exactly those for the larger gasket. In Sec. IV we exploit this property to obtain eigenenergies and functions for a gasket containing 1095 sites by diagonalizing the Hamiltonian on gaskets containing 366 sites.

One more boundary condition is of some interest. Following Ref. 1 once again, we can combine the triangles of Fig. 1 into a periodic lattice. The outside vertices of the triangles are special. Now they have six neighbors, while all other points have four. We describe these special points by an on-site energy $y$. The form of Eq. (17a) and the initial condition $y_n=x_n$ still hold, but now, instead of Eq. (17b), we have

$$g(y,x,\phi)=\frac{y(x^3-3x-2\cos3\phi)-6x(x+\cos3\phi)}{x(x^3-7x-6\cos3\phi)} . \quad (18a)$$

Then, when the last stage is reached, the on-site energy is $y_1$, while the phase is $\phi_1$. In this last stage the system lies upon a triangular lattice. A brief calculation shows that the allowed energies of the lattice are in the range

$$\min_{l=1,2,3} 6\cos\left[\phi+\frac{2\pi}{3}l\right] < x_1 < \max_{l=1,2,3} 6\cos\left[\phi+\frac{2\pi}{3}l\right] . \quad (18b)$$

Thus we find, with this boundary condition, that allowed energies occur in bands.

### C. A note on the zero-field case

The approaches to finding the spectrum described in the preceding section must all be modified if the field is zero. The basic problem can be seen in specializing Eq. (10) to the case $\phi=0$. Then this equation reads

$$x'=\frac{x(x+1)(x+2)(x-3)}{\Gamma^{1/2}\mathrm{sgn}N} ,$$
$$N=(x+2)(x+1) , \quad (19)$$
$$\Gamma=(x+2)^2(x+1)^2 .$$

When $x$ is $-2$ or $-1$, Eqs. (19) have an intractable 0/0 structure. That is why these values of $x$ had to be handled specially in Ref. 1. At $\phi\rightarrow\pm60°$, similar singularities appear at $x=2$ or 1.

However, this difficulty is peculiar to these three special cases of $\phi$. For these $\phi$ values, special attention must be given to the values of $x$ which produce the 0/0 structure. However, for all other $\phi$ values, $\Gamma$ remains positive, no distinguished values of $x$ arise, and the methods outlined in subsection B do give the spectrum.

## III. THE SPECTRUM

### A. Introduction

We now proceed in a semiphenomenological fashion and perform a kind of escape-rate experiment[10] in the $x$-$\phi$ plane. This procedure will help us understand the spectrum of eigenstates.

What we shall do is very simple: We initially distribute points uniformly in a region of the $x,\phi$ plane. We then perform $i$ iterations and see how many and which of the original points remain in the region. In previous experiments of this kind[10] the number of points surviving after $i$ iterations, $n_s(i)$, dropped off exponentially,

$$n_s(i)\sim e^{-\beta i}$$

for large $i$.

The measurement of $n_s(i)$ is interesting because $n_s$ gives information about localization, densities of states, and the fractal character of the spectrum. For the case in which gaskets with the order of $3^i$ sites are combined into

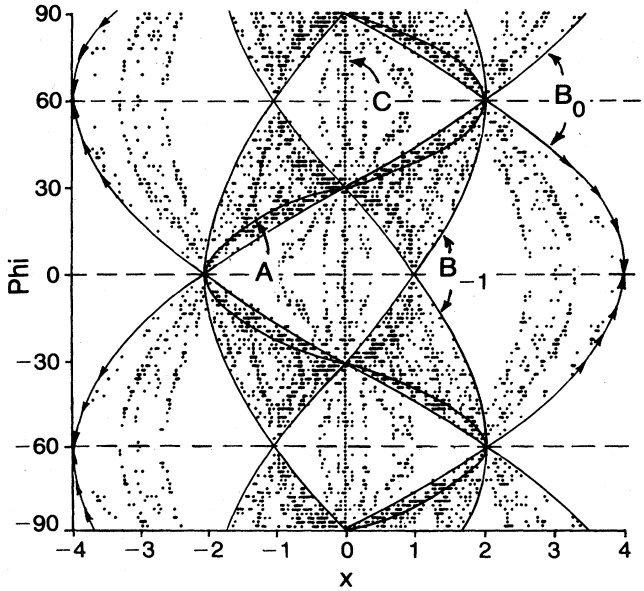


FIG. 4. Set of initial points that do not escape after 100 iterations. Line $A$ corresponds to $x=-2\cos3\phi$. Lines $B$ and $C$ are described in Sec. III C 2.

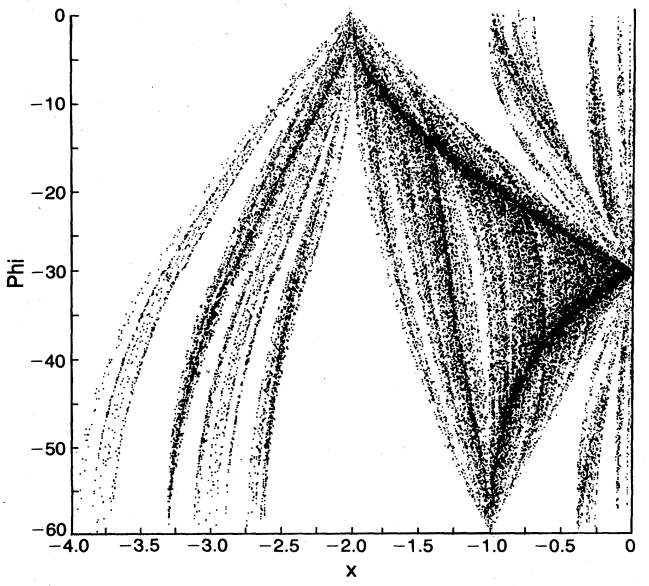


FIG. 5. Set of initial points that do not escape after 300 iterations.

a triangular lattice, $n_s(i)/n_s(0)$ describes the total bandwidth of the spectrum. If $n_s(i)$ decreases exponentially, as in the equation above, $e^{-\beta}$ defines the fractal dimension of the spectrum.

Now look at what happens in our particular example. The first thing to notice is that the spectrum is confined in the interval $-4<x<4$. It is now of particular interest to see how the points in this interval map under application of the recursion as defined in the preceding section. To put things on a more quantitative basis, we discretize the continuum of points in the interval $-4<x<4$, and, say, $-90°<\phi<90°$, into a finite, equally spaced set of points and ask ourselves the following question: Which of these points remain in the interval $-4<x<4$ after, say, $i$ iterations? In Fig. 4 these points are plotted for $i=100$. The initial grid contained $180\times180$ points.

The structure of Fig. 4 is suggestive of a remarkably complicated and rich spectrum of eigenenergies. In Fig. 5 the survivors are plotted for $i=300$, with an initial grid of $240\times240$. This more detailed picture shows the spectrum to consist of a family of lines. Making use of the symmetries displayed in Fig. 4 [the lines $\phi=n\times60°$ are symmetry axes; the points $x=0,\phi=(2n+1)\times30°$ are points of inversion symmetry], the whole $x$-$\phi$ plane can be reconstructed from Fig. 5.

It is interesting to ask what happens at $\phi=0°$. On this line, which maps onto itself, the recursion relation is characterized by the $\lambda=5$ of May-Feigenbaum. A detailed study of the spectrum for this case was presented by Domany *et al.*[1] Figure 5 shows that each point on the $\phi=0$ line corresponds to many lines for $\phi\neq0$. Each line represents an eigenenergy of the system. Hence, setting $\phi=0°$ produces a very considerable degeneracy of eigenvalues and probably a quite different physical behavior.

### B. Escape rate

As a first attempt toward a better understanding of the spectrum of eigenstates, we employ the concept of escape

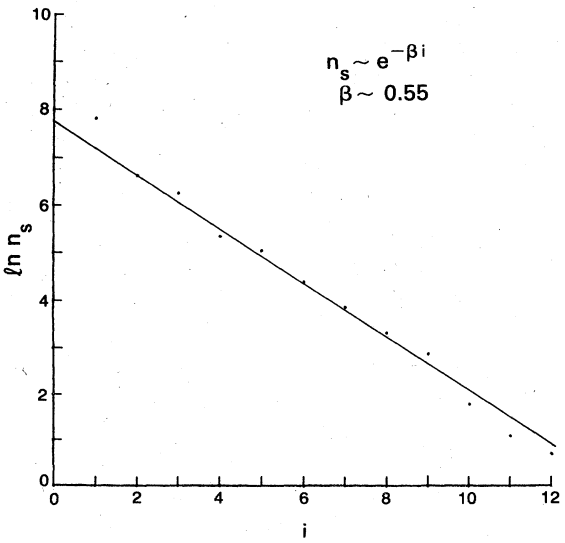


FIG. 6. Plot of the logarithm of the number of survivors vs the number of iterations for the $\phi=0°$ case.

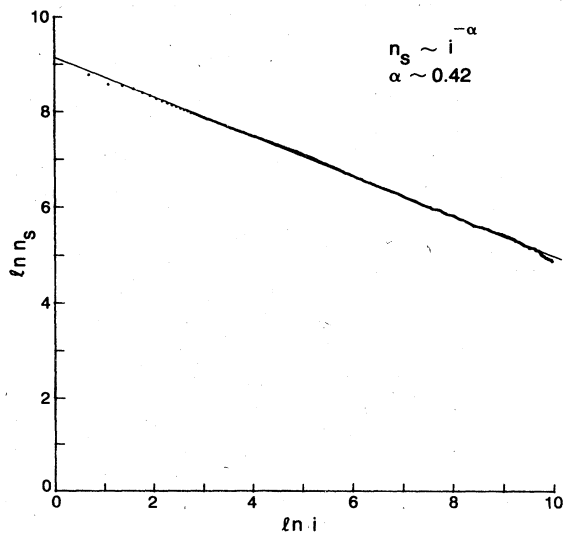


FIG. 7. Log-log plot of the number of survivors vs the number of iterations for $\phi=-10°$. The algebraic law is characterized by an exponent $\sim0.42$.

rate in a more precise manner. Figure 6 is a plot of the logarithm of the number of survivors versus the number of iterations for the $\phi=0°$ case.

As in the cases studied previously,[9,10] $n_s(i)$ decays exponentially. In contrast, consider Fig. 7, which shows the data for $\phi=-10°$ plotted on a log-log scale. After approximately 100 iterations a striking power-law behavior sets in with $n_s(i)\sim i^{-\alpha}$. Here the exponent $\alpha$ is 0.42. We have checked numerically that this exponent is unchanged by small deformations of the region examined in the $\phi$-$x$ plane. The points in Fig. 7 originate from an initial set of 10 000 equally spaced points with $\phi=-10°$ in the interval $-2<x<-1.25$, where, according to Fig. 5, the spectrum is rather dense.

We have also explicitly checked that the escape rate on a triangular lattice made up of gaskets (see Sec. II B) follows the same power-law behavior. It is interesting to note that, within an accuracy of 0.01, the escape-rate exponent is equal to $2-d_f$, where $d_f=\log_{10}3/\log_{10}2$ is the fractal dimension of the gasket. We have not found an explanation for this simple result.

Both exponential and power-law behaviors of the escape-rate rule out the possibility of a continuous spectrum. This is because eventually all of the initially chosen points will disappear towards infinity under repeated application of the recursion relations, and, hence, only a set of measure zero can correspond to eigenstates (due to the fact that the map is "illegal" for these energies, as explained in Sec. II C).

It is intuitively appealing to associate an exponential escape rate with exponentially (or stronger than exponentially) localized wave functions (as, for instance, applies for the case $\phi=0°$); by the same token, the power-law escape rate, as found in this problem, might be suggestive of power-law localized wave functions. However, as we will argue later, the spectrum consists of truly extended wave functions for nonzero $\phi$. The meaning of the escape rate for localization, as such, is still unclear.

### C. More details about the spectrum

The previous numerical experiments establish qualitatively the difference between the one-dimensional (logistic) map for the zero-field problem and the two-dimensional $\phi$-$x$ map for the self-similar-field case. Whereas Figs. 4 and 5 answered the question of which of the initially chosen energies survive after many iterations, the escape-rate experiments, on the other hand, tell us how many survive.

We next deal with the question of where (after many iterations) the survivors actually end up. Numerically, it turns out that all of the survivors get stuck for a long time very close to the line ($A$ in Fig. 4)

$$x=-2\cos 3\phi\ , \tag{20}$$

after which (if one waits long enough) they disappear to infinite energies. This line is clearly visible in Fig. 5 as a very densely packed region of dots.

Indeed, inserting Eq. (20) in the recursion relation for $x$, we find

$$\tilde{x}'=4\tilde{x}(1-\tilde{x}),\quad \tilde{x}=x^2/4\ . \tag{21}$$

This is a "fixed line" characterized by the $\lambda=4$ of May-Feigenbaum. This map is mixing and ergodic; eventually all of the points on this line get visited after an infinite number of iterations. Consequently, the line of Eq. (20) represents a continuum set of eigenstates of the system (i.e., continuously varying with magnetic field or $\phi$).

This line forms the domain of attraction of all the other lines displayed in Fig. 5 (however, see below). We are now in a position to carry out the analysis one step further and see how the map behaves in the linear neighborhood of the fixed line. This then will lead to a qualitative understanding of the numerical data of the preceding sections.

#### 1. Marginal parameter

Let us define the variable

$$Q=\frac{x+2\cos 3\phi}{\sin 3\phi}\ . \tag{22}$$

According to the above, if $Q$ is initially zero it will remain zero. In terms of $\phi$, the recursion relation on the fixed line equals

$$\phi'=-2\phi+\tfrac{1}{2}\pi\,\mathrm{sgn}\phi\ . \tag{23}$$

Apparently, the long escape time is caused, in part, by a trapping near $Q=0$. In particular, if $Q\ll 1$, then

$$Q'=-Q-\tfrac{1}{2}Q^2\tan 3\phi+O(Q^3)\ . \tag{24}$$

That is, $Q$ is conserved for small values of $Q$. Hence, whenever one obtains small $Q$, one will be stuck near the fixed line for a very long time. The marginal behavior of (24) explains the power-law behavior of the escape rates of the preceding sections. For very small values of $\phi$ ($\phi\sim 0.01°$), there is a crossover from an exponential escape rate to the universal algebraic behavior after about ten iterations.

#### 2. Fixed points, lines, and multicycles

Although the foregoing analysis was sufficient to explain our considerations regarding escape-rate phenomena, many of the details of the spectrum are still unknown. This is because the experiments so far have only revealed the domain of attraction of the fixed line of Eq. (20). Other fixed lines or points, having a domain of attraction of one or several dimensions less than that of the fixed line, are very hard to detect. For completeness, we will next give a list of special situations which have been found by trial and error.

Another set of lines which map onto themselves are given by ($B_0$, Fig. 4)

$$x=4\cos(\phi+\xi),\quad \xi=0°,120°,240°\ . \tag{25}$$

The map on these lines is governed by the fixed points ($\phi=0°$, $x=4$) (stable), ($\phi=90°$, $x=0$) (unstable), etc.

Furthermore, they form the boundaries in the $x$-$\phi$ plane of the spectrum and so do their ancestors, i.e., the sequence of lines that ultimately will map onto the lines of Eq. (25). For instance, the lines in Fig. 4 indicated by $B_{-1}$,

$$x=-2\cos(\phi+\kappa),\quad \kappa=0°,150°,300° \tag{26}$$

map, after one iteration, onto $B_0$ [Eq. (25)], and they themselves define boundaries. A sequence of "boundary" lines thus obtained can be regarded as the limit of another (higher-dimensional) sequence of lines which form the domain of attraction of the fixed line of Eq. (20). Already at this level we see that the self-similarity in the spectrum is building up in a very complicated two-dimensional way.

Superimposed on this buildup one has to imagine the existence of multicycles. For example, we found empirically a cycle of length 2,

| $x$ | $\phi$ (rad) |
|---|---|
| −0.729 546 212 | + 0.003 937 949 |
| + 0.272 277 680 6 | −0.014 638 887 |

and one of length 3,

| $x$ | $\phi$ (rad) |
|---|---|
| + 1.732 050 808 | −0.194 444 444 |
| + 1.732 050 808 | + 0.138 888 889 |
| −1.732 050 808 | −0.027 777 778 |

Finally, we mention the lines $[\phi,x]=[\phi,0]$ ($C$ in Fig. 4) and $[\phi,x]=[n\times 60°, x]$, which, as is seen before, map onto themselves.

## IV. PARTICIPATION RATIO

In an attempt to understand the nature of the eigenstates and the distribution of eigenenergies, we have constructed Sierpinski gaskets having up to 365 sites and diagonalized the Hamiltonian numerically. For comparison, we have also carried out similar studies on an Anderson-type model obtained by taking the tight-binding model and adding diagonal disorder distributed uniformly between −0.5 and 0.5. For both calculations, the three different symmetry boundary conditions were used as described in Sec. II B. This enables us to obtain the eigenvalues and eigenstates for a larger gasket, containing 1095 sites with free boundary conditions. From each of the

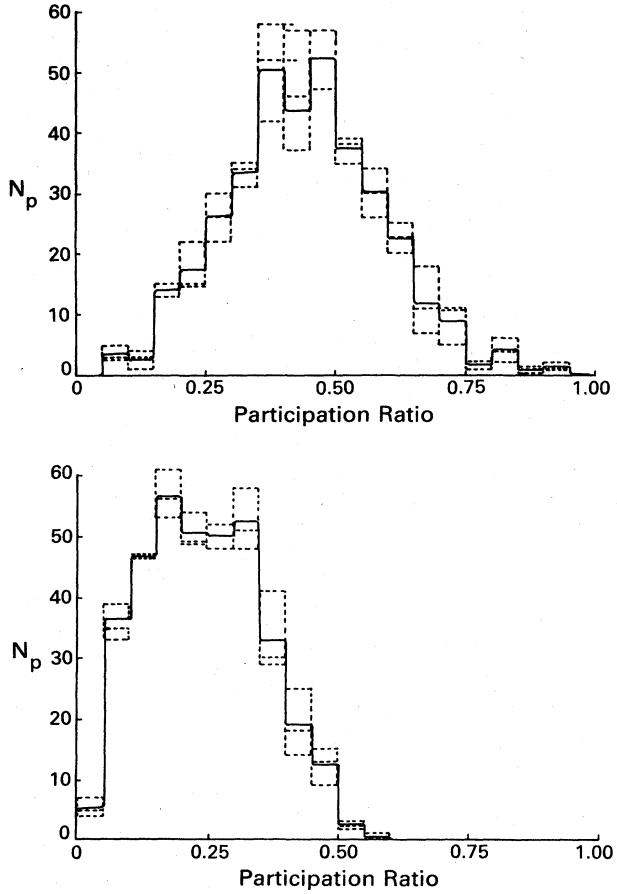


FIG. 8. Histogram of the number of eigenstates $N_P$ having a participation ratio $P$ for a gasket containing 365 sites with three different boundary conditions (dashed curves). The solid curve represents an un-normalized histogram for a larger gasket containing 1095 sites with free boundary conditions. (a) No randomness; $\phi=17°$. (b) On-site randomness uniformly distributed between $-0.5$ and $+0.5$; $\phi=17°$.

eigenfunctions we have calculated the participation ratio defined by

$$p_i=\frac{1}{N\sum_r |\Psi_i(r)|^4} , \tag{27}$$

where $\Psi_i(r)$ is the wave function of the $i$th eigenvalue at site $r$, and $N$ is the total number of sites. For extended states, $p_i$ is of order 1, whereas for localized states, $p_i$ is of order $1/N$.

The results for $\phi=17°$ are summarized in Fig. 8. The effect of disorder is to shift the distribution of participation ratios uniformly to lower values. For the infinite gasket with disorder, the histogram reduces to a $\delta$ function at the origin. Clearly, our finite-size—gasket results do not give conclusive evidence for the true nature of the eigenstates. However, our studies of finite-size effects are not inconsistent with truly extended eigenstates for the gasket without disorder. In the following section we present a more definitive analysis using Green's-function techniques.

## V. ANALYSIS WITH GREEN'S FUNCTIONS

We now return to the generating function formalism of Sec. II. The decimation on the partition function implies a recursion relation for the free energy per site $F=N^{-1}\ln Z$,

$$F=\tfrac{1}{2}b^{-d_f}\ln\Gamma-\tfrac{1}{3}b^{-d_f}\ln D+b^{-d_f}F' , \tag{28}$$

where $D$ and $\Gamma$ are defined in Eqs. (5) and (10), respectively. The density of states can be obtained using

$$\rho(x,\phi)\sim \mathrm{Im}\frac{\partial F}{\partial x} . \tag{29}$$

Hence, the density of states is associated with the zeros in $\Gamma$ and $D$. On the lines $\phi=0°$ and $\phi=60°$, considerable simplification occurs; the recursion relation for the free energy becomes

$$\begin{aligned} b^{+d_f}F&=\ln(x+2)+\tfrac{1}{3}\ln(x+1)\\ &\quad-\tfrac{1}{3}\ln(x-2)+F' \quad \text{for } \phi=0° ,\\ b^{+d_f}F&=\ln(x-2)+\tfrac{1}{3}\ln(x-1)\\ &\quad-\tfrac{1}{3}\ln(x+2)+F' \quad \text{for } \phi=60° . \end{aligned} \tag{30}$$

This recursion relation has been employed in Ref. 3 for the study of the spectrum of eigenstates. For our two-dimensional map, however, the calculation becomes generally intractable. However, we shall proceed to present qualitative arguments regarding the nature of the spectrum. The zeros in $\Gamma$ occur at the points

$$[x,\phi]=[-2,0],[-1,0],[0,30] , \tag{31}$$

and those which can be obtained from these by symmetry. The line described by Eq. (20) passes through two of the points above; this, together with the ergodic property of the $\lambda=4$ map, tells us that the line of Eq. (20) corresponds to a set of eigenstates of the system. As pointed out in Sec. III C, the vast majority of the spectrum maps onto the line of Eq. (20) after successive iterations of the recursion relations. Therefore the nature of the majority of eigenstates is determined by that of the wave functions on the fixed line.

This brings us to the final issue of this exercise, which is to show that the wave functions on this fixed line are truly extended. According to Ref. 1 we can define Green's functions

$$G(r,r')=\langle r\,|\,(x-H)^{-1}\,|\,r'\rangle \tag{32}$$

with simple properties under decimation by taking the lattice sites $r,r'$ to be on the lattice that remains after decimation. Then, after some algebra, one can write the following recursion relation:

$$G(r,r')=D\Gamma^{-1/2}G(R,R') , \tag{33}$$

where $r,r'$ and $R,R'$ denote the same sites on the original and decimated lattice, respectively. On the line $x=-2\cos 3\phi$, the combination $D\Gamma^{-1/2}$ [Eqs. (5) and (10)] reduces to the simple result

$$D\Gamma^{-1/2}=-\frac{\sin 3\phi}{\sin 3\phi'} . \tag{34}$$

We make use of the fact that we are dealing with a point spectrum. This allows us to write, for the Green's function,

$$G^{\pm}(r,r')=\sum_i \frac{\Psi_i^{\dagger}(r)\Psi_i(r')}{x-x_i\pm i0^+} , \tag{35}$$

where the sum is over a discrete set of eigenenergies $\epsilon_i$ and where $\Psi_i$ denotes the corresponding wave functions. In particular, for an eigenvalue on the fixed line we can insert $-2\cos 3\phi$ for $x_i$. From Eqs. (33)—(35) we read off, for the wave functions on that line,

$$g(r,r';\phi)\delta(x+2\cos 3\phi)=-\frac{\sin 3\phi'}{\sin 3\phi}g(R,R';\phi') \times\delta(x'+2\cos 3\phi') , \tag{36}$$

where

$$g(r,r';\phi)\equiv\Psi^{\dagger}(r;\phi)\Psi(r';\phi') , \tag{37}$$

and $\Psi$ denotes the wave function on that line. Note, however, that Eq. (36) can be rewritten as

$$g(r,r';\phi)\delta(Q)=g(R,R';\phi')\delta(-Q') , \tag{38}$$

with $Q$ the marginal field defined in Sec. III C 1. We have thus found a remarkably simple result for the wave functions on the fixed line $A$. Equation (38) implies that $g$ remains unchanged after decimation. Now we can use the fact that the wave functions will change continuously with $\phi$, together with the properties of the recursion relation for $\phi$, Eq. (23), to argue that the spectrum consists of truly extended states. Imagine that $r,r'$ are very far away and denote points on the gasket that will be transformed away only after a very large number of iterations. After each iteration the system acquires a new magnetic field, $\phi$. Since, eventually, after many iterations, the whole $\phi$ interval would have been visited, one can come arbitrarily close to any initial value for $\phi$, if one waits long enough. By continuity, this implies that $g$ is periodic and, hence, the wave functions are extended.

## ACKNOWLEDGMENT

One of us (J.R.B.) is grateful to Jim Roberts for his help with computer graphics.

*Present address: Institute for Advanced Study, Princeton, NJ 08540.

[1]E. Domany, S. Alexander, D. Bensimon, and L. P. Kadanoff, Phys. Rev. B **28**, 3110 (1983).
[2]J. R. Banavar and M. Cieplak, Phys. Rev. B **28**, 3813 (1983).
[3]A. M. S. Tremblay and B. W. Southern, J. Phys. (Paris) Lett. **44**, L843 (1983).
[4]R. Rammal, J. Phys. (Paris) **45**, 191 (1984); Phys. Rev. B **28**, 4871 (1983).
[5]R. Rammal and G. Toulouse, J. Phys. (Paris) Lett. **44**, L13 (1983).
[6]S. Alexander, Phys. Rev. B **27**, 1541 (1983).
[7]R. Rammal and G. Toulouse, Phys. Rev. Lett. **49**, 1194 (1982).
[8]S. Alexander (unpublished).
[9]M. Widom, D. Bensimon, L. P. Kadanoff, and S. J. Shenker, J. Stat. Phys. **32**, 443 (1983).
[10]Leo P. Kadanoff and Chao Tang, Proc. Nat. Acad. Sci. (U. S. A.) **81**, 1276 (1984); M. Kohmoto, L. Kadanoff, and C. Tang, Phys. Rev. Lett. **50**, 1870 (1983).
[11]R. May, Nature (London) **261**, 459 (1978).
[12]M. Feigenbaum, J. Stat. Phys. **19**, 25 (1978).
[13]Y. Gefen, A. Aharony, Y. Shapir, and B. B. Mandelbrot, J. Phys. A **17**, 435 (1984).